LLNL-JRNL-490846

Establishment of rules for interpreting ultraviolet autofluorescence microscopy images for non-invasive detection of Barrett's esophagus and dysplasia

S. G. Demos, B. Lin, S. Urayama, R. M. G. Saroufeem, D. L. Matthews

July 15, 2011

Journal of Biomedical Optics

Establishment of rules for interpreting ultraviolet autofluorescence microscopy images for non-invasive detection of Barrett's esophagus and dysplasia

Bevin Lin[1,2], Shiro Urayama[3], Ramez M. G. Saroufeem[4],

Dennis L. Matthews[1,2], Stavros G. Demos[1,5]

[1]University of California, Davis NSF Center for Biophotonics Science & Technology, 4800 2nd Avenue, Sacramento, CA 95817

[2]University of California, Davis Department of Biomedical Engineering, One Shields Avenue, Davis, CA 95616

[3]University of California, Davis Medical Center, Division of Gastroenterology and Hepatology, 4150 V Street, Suite 3500, Sacramento, CA 95817

[4]University of California, Davis Medical Center, Department of Pathology, 4400 V Street, Sacramento, CA 95817

[5]Lawrence Livermore National Laboratory, 7000 East Avenue, Livermore, CA 94550

ABSTRACT

The diagnostic potential of autofluorescence (AF) microscopy under UV excitation is explored using *ex vivo* human specimens. The aim is to establish optical patterns (the rules for interpretation) that correspond to normal and abnormal histologies of the esophagus spanning from early benign modifications (Barrett's esophagus) to subsequent dysplastic change and progression towards carcinoma. This was achieved by developing an image library categorized by disease progression. We considered morphological changes of disease as they are compared to histological diagnosis of the pathological specimen as well as control samples of normal esophagus, proximal stomach, and small

intestine tissue. Our experimental results indicate that UV AF microscopy could provide real-time histological information for visualizing changes in tissue microstructure that are currently undetectable using conventional endoscopic methods.

INTRODUCTION:

Although the pathogenesis of esophageal adenocarcinoma (EAC) is still unclear, [1-2] there is a general consensus among the medical and research community that the increasing rate of gastroesophageal reflux disease (GERD) has contributed to the annual increase of EAC incidence of more than 20% since 1975.[3-4] The associated mortality of EAC has increased more than seven times during the period, faster than any other malignancy in the United States.[5] GERD affects at least 15-20% of the adult population every week,[4, 6] and 7-10% of the GERD population may suffer from chronic injury to the distal esophagus with a consequence of metaplastic changes in the distal esophageal lining,[3-4, 7-8] a condition referred to as Barrett's esophagus (BE).

BE is considered a premalignant condition where the stratified squamous epithelium of the distal esophagus is replaced with specialized intestinal epithelium – columnar epithelium containing goblet cells.[1, 9] Current definition of BE requires both endoscopic documentation of presence of glandular epithelial lining and the histological identification of specialized intestinal metaplasia with goblet cells, the hallmark of BE[1] in esophagus.[10] Apart from repeated endoscopy and multiple biopsies, there is no definite method of evaluating accurately which patients with BE are progressing into dysplasia and ultimately carcinoma, though patients with long segment, long standing BE are more likely to demonstrate progression to dysplasia/carcinoma. Recent studies suggest the GE junction to be the site of metaplastic initiation, starting with the distal esophageal squamous mucosa being replaced by columnar epithelium similar to that seen in the gastric cardia.[9, 11] This columnar mucosa of the distal esophagus has been histologically found to contain undetected BE in 15-24% of an endoscopically normal junction.[11] From a practical standpoint, this percentage may reflect the endoscopic appearance of the velvety-salmon texture-discoloration (suggestive of columnar-lined epithelium), which could be subjective and subtle. It should be noted, however, that the presence of intestinal metaplasia in the cardia (or any part of the stomach) is managed differently from BE patients.

The risk of BE patients developing cancer is divided into four histopathological categories; no dysplasia, indefinite for dysplasia, low grade dysplasia (LGD), and high grade dysplasia (HGD).[9, 12] The histological pretreatment classification determines clinical management of the patient and often suffers from poor inter-observer agreement.[13] For late stage dysplastic lesions within the mucosa, local endoscopic management such as mucosal resection or ablation techniques have demonstrated efficacy without significant morbidity.[14-19] Thus, providing accurate histological diagnosis becomes critically important for identification of the clinical decision point for early endoscopic intervention.

Dysplasia classification for pretreatment diagnosis is generally taken from the Vienna classification system[20-21] or has historically been transposed from criteria that define inflammatory bowel disease.[12, 21] The histologic criteria used as reference in this work has been adopted from literature sources.[7, 9, 12-13] This compiled "Pathology Diagnosis" is defined in column 1 of Table 1, "Histological Architechture" and "Cytology" are summarized in columns two and three, and column 4 outlines the "Optical Image Morphology", the rules of interpretation from which the work herein describes. These defining cellular features are essentially invisible to the endoscopist at the time of biopsy specimen collection. A positive biopsy sampling of dysplasia is thus commonly obtained randomly and subject to the previously mentioned inter-observer variability. These are two of the greatest challenges when providing optimal care to patients with BE.[12-13] LGD, the earliest sign of malignant progression, has the least consistent agreement and lowest reproducibility between pathologists.[12, 21-22] The standard option for physicians is to wait until HGD is identified at surveillance endoscopy procedures before electing for endoscopic or surgical treatment for the esophagus.[7] Research using confocal microscopy[23-24] has provided promising results toward real-time histology, generating a 'Confocal Barrett's Classification' system.[25-26] This approach, however, requires application of contrast agents. Nonlinear excitation and frequency conversion microscopy imaging techniques do not require contrast agents but generally require complex instrumentation.[27] It has recently been demonstrated that AF microscopy under UV excitation provides visualization of cellular morphology and organization in *ex vivo* esophagus specimens using no contrast agents or tissue preparation.[28] Due to the short propagation depth of UV excitation, the AF signal is confined in the epithelium, allowing for acquisition of high-resolution images using high signal collection efficiency designs such as wide field microscopy. This in turn allows image acquisition at clinically relevant exposure doses using only the tissue's native fluorescence.[29]

In this work, we present *ex vivo* results of autofluorescence microscopy under UV excitation from the esophagus, the stomach, and the intestine in order to establish optical patterns (rules of interpretation) that correspond to normal and abnormal histologies of the human esophagus and its transformation to BE with subsequent dysplastic changes and progression to carcinoma. The results suggest that application of this method in a clinical setting could provide diagnostic information in real time which could be used by physicians as a tool to perform targeted biopsy/therapy, and to obtain biopsy specimens that more accurately represent the disease.

MATERIALS AND METHODS

Patient Enrollment and Tissue Sample Collection

Eligible patients were identified and consented at the time of endoscopy by the study clinical investigators. The study protocol utilized was approved by the University of California, Davis Medical Center (UCDMC) Institutional Review Board. Fifty-six patients undergoing routine surveillance endoscopy for Barrett's esophagus, dysplasia, and suspected esophageal cancer were enrolled in this clinical study. Four biopsy specimens were collected per patient for a total of 224 tissue samples. Biopsy specimens were collected with standard forceps and placed individually in labeled sterile containers with RPMI1640 media (Invitrogen, Carlsbad, CA). The first tissue biopsy specimen was taken from the proximal stomach (cardia). This was important in order to establish optical morphology of cardia mucosa as a control, as well as to rule out cardia adenocarcinoma.[7, 12] The second control biopsy specimen was taken from the descending small intestine (duodenum). The third endoscopic biopsy specimen was taken from the distal esophagus and considered as the pathological sample. The fourth biopsy specimen was taken from above the Z-line (squamocolumnar junction), in the squamous epithelium of the esophagus and was documented to be the normal esophageal control sample. Immediately after image processing, each biopsy specimen was placed in 10% formalin for fixation and transferred to pathology for tissue diagnosis. Each tissue biopsy specimen was taken to be histopathologically homogeneous such that the AF images were representative of the pathology diagnosis. The pathological evaluation was confirmed by at least two expert pathologists and taken as the diagnostic gold standard from which the optical images were categorized.

Optical Imaging Protocol

Each tissue sample was placed on a standard pathology cassette without preparation and minimal handling. The tissue sample was covered with a quartz slide for imaging. The microscope imaging prototype platform was previously described in detail.[30] In brief, a compact diode-pumped solid-state laser operating at 266 nm (Intelite, Inc., Minden, NV) was used as the photo-excitation source to generate the AF images. The resulting AF images arose predominantly from the emission of tryptophan[31] and provide a representation of the structure of the top layer of tissue cells (imaging depth of less than about 50 μm). The microscope system was equipped with a 20X long working distance objective followed by a 5X zoom lens. The images were recorded using a liquid nitrogen cooled charge-coupled device (Princeton Instruments, Inc., Trenton NJ).

Approach for developing rules of interpretation.

The images of the specimens in this study were compiled into a preliminary image gallery of normal and abnormal tissue structure that could be used to establish a correlation between image morphology and histopathology. We hypothesized that progression of abnormality was associated with the severity of deviation from normal structures observed in the UV AF images. Since BE required the presence of goblet cells, we included in our study imaging of normal intestinal specimen in order to establish the morphology of goblet cells (normally present in the intestine) to enable comparison with features observed in the images of BE. The intestine structure was also associated with the presence of villi and crypts, which were important recognition factors in the AF images. Furthermore, as the gastric type cellular morphology near the GE junction was shown to be associated with metaplastic progression, we included normal stomach tissue in this imaging study. Consequently, the analysis and categorization of the images for developing optical pattern recognition rules related to their histopathological state was focused on distinguishing: a) normal esophageal tissue, b) normal stomach and intestine tissue, c) BE with no dysplasia, and d) BE with dysplasia and cancer. Typical examples for each of these categories and results will be presented next in separate subsections

RESULTS

Nondysplastic esophageal columnar and normal squamous epithelium control images

The H&E staining of nondysplastic esophageal columnar mucosa section shown in Fig. 1a demonstrates the typical honeycomb pattern observed in this type of tissue. A typical microscopic UV AF image captured from specimens of normal columnar mucosa is shown in Fig. 1b. This image demonstrates visualization of the honeycomb pattern of the cells showing their outlines with higher intensity compared to the cytoplasm region.[32] The nuclei of the cells that appear as tile-like structures can be appreciated as darker features in the image of an H&E stained section of normal esophageal squamous epithelium, shown in Fig. 2a. The microscopic UV AF images of squamous epithelium, illustrated in Fig. 2b, showed the same characteristic appearance as Fig. 2a, clearly outlining individual cells and nuclei. These well recognizable patterns observed in the UV AF images shown in Figs. 1b and 2b represent the characteristic morphology of the normal stratified squamous and columnar esophageal mucosa observed in fresh unprocessed specimens obtained without any tissue preparation. These typical examples of our observations were considered as the baseline (control) images for normal (healthy) esophageal tissue.

Normal intestinal and gastric epithelium control images

The UV AF images shown in Fig. 3 represent typical examples of our results obtained from human biopsy specimens from normal duodenum (intestine) mucosa (Fig. 3a) and normal cardia (proximal stomach) mucosa (Fig. 3b). Due to the use of the quartz slide on top of the specimen during imaging to slightly compress the tissue in order to achieve a flatter surface, the villi seen throughout this image are also compressed and appear as round structures. Line 1 in Fig. 3(a) is pointing towards three such round structures that represent villi apices within the AF image of normal duodenal mucosa. The center apex had an approximate diameter of 40-50 µm. Similar rounded features were visible throughout the luminal surface. The height of the villi typically varies from 0.5 to 1 mm while their diameters vary from approximately one-eighth to one-third of their height. Although the villi were compressed during imaging (to help better indentify the goblet cells), their outlines are clearly visible within the image of Figure 3a and their observed diameter is within the normal parameters.

As discussed earlier, it is important to recognize and optically identify goblet cells in the AF images of the intestine. The nucleus of goblet cells is at their base along with the organelles, while the remainder of the cell is filled with membrane-bound secretory granules filled with mucin. The "goblet cell" name comes from their cup-like shape. As goblet cells produce mucin, it was necessary to consider the different imaging results that mucin might produce if it is present inside the goblet cells of the fresh tissue biopsy specimens during AF imaging. Our experimental results strongly suggested that mucin typically produced an increased AF signal compared to the AF of the cells. Therefore, goblet cells containing mucin produced a much higher intensity than goblet cells without mucin within the fresh tissue, and served as an optical guideline documented in Table 1. These observations are illustrated with lines 2 and 3 in the AF image of normal duodenum, shown in Fig. 3a. A dark and a bright feature are indicated respectively, each with a diameter of approximately 11 µm. We assume that the dark feature was a goblet cell with no mucin while the bright feature is a goblet cell containing mucin. Similar features to those identified above could be found in the image shown in Fig. 3a and in similar images of normal intestine tissue. Thus, the results suggested that the goblet cells could be observed in the microscopic UV AF images as bright or dark features, on the order of 10 μm in diameter, depending on the mucin content at the time of imaging. Finally, line 4 points to two similar features that were believed to represent crypts of Lieberkuhn of the duodenal epithelium.

The microscopic UV AF image of cardia mucosa shown in Fig. 3(b) was representative of such images obtained from normal stomach epithelium specimens. The normal duodenum and cardia mucosal images such as those shown in Fig. 3 provided the control images to exemplify what microstructures of interest would look like using this imaging methodology. These AF images could be used as a baseline for comparison with images of specimens presenting benign intestinal metaplasia modifications of the esophagus indicating Barrett's esophagus, (BE) as discussed in the next section.

Visualization of benign epithelial modifications

Fig. 4 presents an esophagus biopsy specimen AF image that was collected at the endoscopically observed GE junction. The AF image of the distal esophagus in Fig. 4 showed polypoid-like projections, which look more similar to the gastric mucosa of Fig. 3(b) than the squamous mucosa shown in Fig. 2(b) or the columnar mucosa shown in Fig. 1(b). Histologically unremarkable squamous esophageal mucosa with very scant columnar components was given as the pathological diagnosis for the case associated with the specimen shown in Fig. 4. The scant honeycomb pattern was preserved in the columnar mucosa, similar to that shown in Fig. 1(b). The irregular polypoid surface appeared to be transitioning from squamocolumnar mucosa containing villi crypts (arrows), consistent with previous results.[31] The multiple projections might be seen as unfolding areas with glands, obscuring the flat surface of stratified squamous mucosa, and inhibiting a clear focus of features beneath the structures of greatest height. We commonly observed that optical images of cardia-type mucosa as those seen in Fig. 4, which appear at first glance to be modified from the characteristic morphology of the nondysplastic or normal esophageal tissue shown in Figs 1 and 2, but were not yet differentiated EAC as shown in Fig. 8 below. However, patient history must be considered when examining diagnostic results related to disease progression, especially for those on chronic medication. Many BE patients are placed on proton pump inhibitors (PPI) in an attempt to reduce associated acid reflux. PPI therapy is associated with several histological changes including parietal cell and foveolar hyperplasia, as well as microcystic dilation of gastric glands. This transformation is a common observation in GE biopsies of the cardia mucosal cells. These surface nodularities, identifiable with UV autofluorescence microscopy, possibly correspond to the above described PPI effect seen histologically and shown in Fig. 4. This could explain the commonly observed nodularity in the squamous esophageal mucosa in our study, which is reminiscent of fundic gland polyps generally seen in the gastric body in patients with BE on PPI therapy. Consequently, this UV AF method provides a clinically important distinction of normal gastric columnar mucosa that standard endoscopy is generally limited from distinguishing.

Visualization of Barrett's esophagus (benign modifications)

Figure 5a shows the H&E gold standard cross-sectioned image of an esophagus specimen from a patient with pathology diagnosis of BE with mild to moderate chronic inflammation and suspected LGD. This esophagus biopsy specimen was collected at 32 cm with an unlisted Z-line and GE junction. The UV AF image shown in Fig. 5b is of the same esophagus biopsy specimen shown in Fig. 5a. It should be considered for correlation purposes that image features viewed from the surface with AF microscopy (top view) varied in diameter from H&E section (cross sections of the biopsy specimen). The suspicion of LGD in Fig. 5(a) was histopathologically defined by the closely packed overlapping basal nuclei with hyperchromasia and irregular contours of H&E surface morphology, although the overall epithelial architecture appeared to be preserved maintaining a degree of uniformity at the surface. Arrows 1 and 2 pointed to goblet cells approximately 10-15 μm in diameter. The goblet cell indicated by arrow 1 was contained within a crypt of Lieberkuhn gland (arrow 3) that was approximately 313 μm along the horizontal axis. Arrow 4 indicated a gland that had become inflamed and angulated, resulting in visible architectural distortion; only the lower portion is remaining resulting in an apparent triangular shape instead of the normal donut shape. This distorted and inflamed gland was approximately 104 μm in diameter with the villi apex beginning to project from the mucosa surface, possibly becoming further distorted during tissue biopsy removal. The cluster of four glands approximately 200 μm sub-surface might attribute to the irregular contours at the surface visible in Fig. 5(b). Fig. 5(b) presents the luminal-plane AF image with numerical arrows corresponding to the same numbered arrows in the H&E image of Fig. 5(a). Based on the criteria for the recognition of goblet cells in the AF images presented in the previous section, arrows 1 and 2 in the AF image of this specimen were believed to be the UV AF optical representation of goblet cells each with a diameter of about 10 µm. Surface features in the UV AF image can be correlated with the 313 µm in diameter crypt of Lieberkuhn gland indicated by arrow 3. This feature had a target-like appearance with light and dark alternate rings and a diameter of approximately 30 – 35 µm. Similar features were observed in other locations in the same figure. Based on previous observations in various specimens, we hypothesize that the dark center represented the opening of a crypt towards the lumen of the gland [31], shown with line 4 in Fig. 3a. The inconsistency of visibility could be attributed to the difference of height projection of villi into the luminal plane. Arrow 4 may indicate the gland that had become inflamed and angulated, resulting in visible architectural distortion from both the AF epithelial surface as well as the H&E image (Fig. 5(a) arrow 4).

The AF images shown in Fig. 6 were from two different patients and represented the images obtained from specimens with varying grades of BE. The biopsy specimen shown in Fig. 6a was collected at 39 cm (GE junction unlisted) and returned a pathology report of BE with reactive atypia. The biopsy specimen shown in Fig. 6b was collected at 32 cm, 1 cm above the Z-line (33 cm), with a GE junction located at 35 cm and returned a pathology report of BE with moderate acute and chronic inflammation, indefinite for dysplasia. The optical features within the honeycomb structure (defined in Fig.1), were previously assigned to represent villi, crypts, and goblet cells of the small intestine (see Fig. 3), and can be easily recognized with the progression to BE throughout the esophagus AF images shown in Fig. 6. For example, a large dark feature that may represent villi apices is indicated with line 1 in Fig. 6(a). Villi may not be immediately apparent because a regular villous appearance was not always a characteristic of BE as it is of the duodenum. Line 2 in Fig. 6(b) indicates a feature slightly smaller than the feature of line 1 that is consistently seen scattered throughout a honeycomb background. These features could be the formation of crypts of Lieberkuhn as in Fig. 3(a). Dark and bright features were also visible and could be correlated to non-mucin and mucin filled goblet cells, lines 3 and 4 respectively. The surface of the columnar mucosa in Fig. 6(b) retained a degree of normality and smoothness, an indication that dysplasia had not yet developed. The categorization of “indefinite for dysplasia” might not be visible from the surface epithelium as this histologic abnormal progression was diagnosed using a traditional cross-section of tissue on a slide.

Low grade dysplasia in BE

The esophagus AF images shown in Fig. 7 were from three different patients with a pathological diagnosis of LGD. The optical features of what are believed to represent villi, crypts, and goblet cells (defined in previous sections) could be recognized throughout Fig. 7. For example, the image of Fig. 7(a) has a very similar appearance to the BE images of Fig. 6 above. This biopsy specimen was collected from 34 cm just above the GE junction at 35 cm. The villi appear to maintain a degree of regularity as they are seen projecting from the surface epithelium. It is also possible that the rounded features are cardia-type mucosa biopsied near the top of a hiatal hernia. There is a cloudy region in the upper right with bright streaks that might be a layer of mucous or vasculature, appearing to overlay the luminal surface. The images of the tissue biopsy specimens shown in Fig.s 7(b) and (c) have visible projections that obscure the flat surface of normal mature squamous epithelium exemplified in Fig. 2(b). The overall surface pattern in the lower half of Fig. 7(b) appears to remain intact. The biopsy was collected from 36 cm. The snaking pattern in the upper half of Fig. 7(b) might represent the formation of pseudostratification extending to the surface, a cytology hallmark of LGD. The bright streaks across the center might indicate vascularization from injury or recovery from previous radio-frequency (RF) ablation therapy. Villi that appear to be forming in the lower half of Fig. 7(c) maintained a regular appearance more similar to those of the duodenum in Fig. 3(a). The Z-line was at 39 cm and the GE junction was at 40 cm, the location of biopsy specimen collection. The image was increasingly out of focus as the surface becomes more three-dimensional as opposed to the pavement-like surface of stratified squamous epithelium shown in Fig. 2(b).

High grade dysplasia and esophageal adenocarcinoma

Figure 8 illustrates UV AF images of HGD and EAC. It can be easily appreciated that these images exhibit a high degree of deviation from the normal esophagus epithelium shown in Fig. 2(b). All of the images had an increasingly disorganized three dimensional aspect, the characteristic complex mucosal architecture, and villiform configuration that currently defines HGD and EAC. Each esophagus biopsy specimen shown in Fig. 8 was taken from different patients. The UV AF image shown in Fig. 8(a) was obtained from a biopsy specimen with pathological diagnosis of squamocolumnar mucosa with HGD. This image depicts three dimensional globular features visible on the mucosal surface and reflective of HGD causing a villous topography and crowding discussed in more detail later. Fig. 8(b) was obtained from a specimen with pathological diagnosis of focal adenocarcinoma in a background of high and low grade dysplasia. The villiform surface and disorganized mucosal pattern could definitively be differentiated from the stratified squamous epithelium of normal esophagus shown in Fig. 2. Mucosal crowding and disorganization were visible in the AF image and correlated with pathological assessment. Villiform features were visible as cauliflower-like projections, 10-30 μm in diameter, and corresponded to malignant features observed in the H&E section of this specimen. Features that correspond to goblet cells with a diameter of approximately 15 μm were also visible along with the crypts. Pathological diagnosis of EAC with similar image characteristics displaying an increasingly villiform surface and a disorganization of mucosal pattern can also be recognized in the images shown in Figs. 8c & d. In Fig. 8d, the pathological diagnosis was poorly differentiated adenocarcinoma. Margin delineation capability is exemplified, as the tissue on the left of the image resembled squamous mucosa shown in Fig. 2(b), while the tissue to the right of the image had more of a continuous mucosal and a cribiform growth patterns similar to the pathologically diagnosed EAC shown in Fig. 8c. There is a visible decrease of pattern regularity with progression of disease observed as tissue transitions from HGD (see Fig. 8(a)) to EAC (see Fig. 8(b-d)). Additionally, EAC was characterized by the proliferation of small irregular glands that contributed to the overall cauliflower-like appearance that was especially visible in Figs. 8(b) and (c). Currently it is extremely difficult to differentiate HGD and EAC,[12] and histologic criteria that defines a diagnosis of intramucosal cancer has not yet been published.[13] In Fig. 8(a), the three dimensional round features represented nodularity of the surface epithelium that might also imply an early onset of carcinoma. Figs 8(b) and (c) both demonstrated a cauliflower-like appearance than HGD, indicating EAC. These optical rules for interpretation are tabulated in Table 1 below in the "Optical Image Morphology" column.

DISCUSSION

Recent work has shown that the gastroesophageal (GE) junction harbors the first stages of intestinal metaplasia.[9, 11] Arguably, providing an imaging technology that identifies goblet cells *in vivo* (such as the technique presented in this work) would allow for early detection of intestinal metaplasia within columnar (non-squamous) mucosa of the distal esophagus. Identification of goblet cells becomes less meaningful when dysplasia or cancer is detected. Technology that can identify microscopic dysplastic changes would enable biopsy specimens to be collected in suspiciously abnormal regions, compared to current practice of random biopsy. This is particularly important in long segment BE which currently necessitates time consuming multiple biopsies to ensure adequate sampling.

The imaging approach presented in this work provides visualization of morphological changes of the epithelial layer where 85% of all cancers initiate.[33] The goal of this work was to explore the potential of this method to provide real-time histological information that does not rely on contrast agents or other type of tissue preparation. We postulate that this approach may have associated savings in cost and time, which are especially critical during an upper endoscopy when the duration of the procedure can be very short. The UV AF images of mucosal biopsy specimens presented in this work are evaluated based on their pretreatment classification which is the gold standard of BE diagnosis.[21] The results of our study suggest that this method may have a high degree of impact at the end points of dysplastic staging where pathology has yet to be defined. Histopathologic criteria for LGD and HGD have been proposed and documented in numerous publications and text books in the medical literature, yet the differentiation between LGD and HGD associated with BE has been a source of diagnostic discrepancy even amongst specialized expert GI pathologists, associated with low inter- and intra-observer reproducibility. Quantification of optically visable observations may provide the fingerprint for defining the end points of dysplasia by simultaneously providing targeted biopsy to the endoscopist and reducing inter-observer variability. Therefore, interpretation of the images provided with this method can be achieved using the classical knowledge of disease progression without a need to develop an entirely new set of approaches for the interpretation of the images. Based on our preliminary findings, we have developed a preliminary set of rules for the interpretation of the UV AF images that are summarized above in column 4 of Table 1, "Optical Image Morphology".

Analogous to the 'Confocal Barrett's Classification', this set of rules serves as a foundation from which to build on.[25-26] As it has taken decades to correlate abstract images of stained tissue sections and establish traditional histology, a similar effort may be needed to establish the correlation of characteristic features observed in the images obtained using new technologies such as the UV AF microscopy method discussed in this work. It must be noted that this method is insensitive when disease characteristics lack appearance or alteration of epithelial features. One such example is the case of "indefinite for dysplasia" which lacks changes in the surface epithelium making evaluation of surface maturation difficult.[21] Mucosal features are a critical guideline for both optical imaging and the pathologist's evaluation of the presence or absence of surface maturation, an important feature that helps to determine regeneratory versus dysplastic changes.[21]

From 1998 to 2005, esophageal disorder related hospitalizations increased by 216% with associated costs increasing by 289%.[34] It has been acknowledged that the current tradition of collecting random biopsy specimens and classifying these samples using a method fraught with variability reduces the chance of finding a curable neoplasia to chance.[7, 35] 30% of endoscopic resection cases have recurrent neoplasia due to missed segments of disease during endoscopy, and 40-60% of patients may already have an invasive malignancy by the time a biopsy specimen accurately reveals high grade dysplasia to the pathologist.[36-37] A reduction of biopsied tissue for preparation and reading would save drastically in both cost and time, as well as improve the patient quality of life. Thus, an endoscopic imaging system that provides real-time histology of early esophageal disease without the additional cost of contrast agents or preparation time has a potential cost saving comparable to breast cancer screening (mammography) and cervical cancer screening (Pap smear).[38] The change of traditional methods comes with the challenge of implementing and interpreting histology-like optical images. The adaptation of new technology will depend on producing highly reproducible, specific, and sensitive information that correlate with the familiar and established guidelines of disease diagnosis.

ACKNOWLEDGEMENTS

This work performed in part under the auspices of the U.S. Department of Energy by Lawrence Livermore National Laboratory under Contract DE-AC52-07NA27344. This research is supported by funding from the Center for Biophotonics, an NSF Science and Technology Center, managed by the University of California, Davis, under Cooperative Agreement No. PHY 0120999.

REFERENCES

1. N. J. Shaheen, and J. E. Richter, "Barrett's oesophagus," *Lancet* **373**(9666), 850-861 (2009)
2. P. Enzinger, and R. Mayer, "Esophageal cancer," *N. Engl. J. Med.* **349**(23), 2241-2252 (2003)
3. I. Qureshi, M. Shende, and J. Luketich, "Surgical Palliation for Barrett's Esophagus Cancer," *Surg. Oncol. Clin. N. Am.* **18**(3), 547-560 (2009)
4. M. Pera, C. Manterola, O. Vidal, and L. Grande, "Epidemiology of esophageal adenocarcinoma," pp. 151-159 (2005).
5. H. Pohl, and H. Welch, "The role of overdiagnosis and reclassification in the marked increase of esophageal adenocarcinoma incidence," *JNCI Cancer Spectrum* **97**(2), 142 (2005)
6. N. Shaheen, and D. Ransohoff, "Gastroesophageal reflux, Barrett esophagus, and esophageal cancer: scientific review," *JAMA* **287**(15), 1972 (2002)
7. K. J. Lewin, R. Riddell, H., and W. Weinstein, M., Gastrointestinal Pathology and Its Clinical Implications, IGAKU-SHOIN Medical Publishers, Inc. (1992).
8. S. Spechler, J. Zeroogian, D. Antonioli, H. Wang, and R. Goyal, "Prevalence of metaplasia at the gastro-oesophageal junction," *The Lancet* **344**(8936), 1533-1536 (1994)
9. J. H. Peters, T. J. Watson, and T. R. DeMeester, "Esophageal Anatomy and Physiology and Gastroesophageal Reflux Disease," in Greenfield's Surgery: Scientific Principles and Practice, pp. 674-677, Lippincott Williams and Wilkins (2006).
10. J. Lenglinger, B. Izay, M. Eisler, F. Wrba, J. Zacherl, G. Prager, and F. Riegler, "Barrett's esophagus: Size of the problem and diagnostic value of a novel histopathology classification," *European Surgery* **41**(1), 26-39 (2009)
11. J. Lenglinger, M. Eisler, F. Wrba, G. Prager, J. Zacherl, and M. Riegler, "Update: histopathology-based definition of gastroesophageal reflux disease and Barrett's esophagus," *European Surgery* **40**(4), 165-175 (2008)
12. T. Rice, W., J. E. Mendelin, and J. R. Goldblum, "Barrett’s Esophagus: Pathologic Considerations and Implications for Treatment " *Semin. Thorac. Cardiovasc. Surg.* **17**(4), 292-300 (2005)

13. E. Downs-Kelly, J. E. Mendelin, A. E. Bennett, E. Castilla, W. H. Henricks, L. Schoenfield, M. Skacel, L. Yerian, T. W. Rice, L. A. Rybicki, M. P. Bronner, and J. R. Goldblum, "Poor Interobserver Agreement in the Distinction of High-Grade Dysplasia and Adenocarcinoma in Pretreatment Barrett's Esophagus Biopsies," *Am. J. Gastroenterol.* **103**(9), 2333-2340 (2008)
14. G. Y. Lauwers, D. G. Forcione, N. S. Nishioka, V. Deshpande, M. Y. Lisovsky, W. R. Brugge, and M. Mino-Kenudson, "Novel endoscopic therapeutic modalities for superficial neoplasms arising in Barrett's esophagus: a primer for surgical pathologists," *Mod. Pathol.* **22**(4), 489-498 (2009)
15. H. Mork, O. Al-Taie, F. Berlin, M. R. Kraus, and M. Scheurlen, "High recurrence rate of Barrett's epithelium during long-term follow-up after argon plasma coagulation," *Scand. J. Gastroenterol.* **42**(1), 23-27 (2007)
16. S. Wani, S. R. Puli, N. J. Shaheen, B. Westhoff, S. Slehria, A. Bansal, A. Rastogi, H. Sayana, and P. Sharma, "Esophageal Adenocarcinoma in Barrett's Esophagus After Endoscopic Ablative Therapy: A Meta-Analysis and Systematic Review," *Am. J. Gastroenterol.* **104**(2), 502-513 (2009)
17. M. I. Canto, K. B. Dunbar, P. Okolo, S. B. Jagannath, and S. V. Kantsevoy, "Low flow CO2-cryotherapy for high risk Barrett's esophagus (BE) patients with high grade dysplasia and early adenocarcinoma: A pilot trial of feasibility and safety," *Gastrointest. Endosc.* **67**(5), Ab179-Ab180 (2008)
18. S. R. DeMeester, "New options for the therapy of Barrett's high-grade dysplasia and intramucosal adenocarcinoma: Endoscopic mucosal resection and ablation versus vagal-sparing esophagectomy," *Ann. Thorac. Surg.* **85**(2), S747-S750 (2008)
19. V. Sharma, K. Wang, B. Overholt, C. Lightdale, M. Fennerty, P. Dean, D. Pleskow, R. Chuttani, A. Reymunde, and N. Santiago, "Balloon-based, circumferential, endoscopic radiofrequency ablation of Barrett's esophagus: 1-year follow-up of 100 patients," *Gastrointest. Endosc.* **65**(2), 185-195 (2007)
20. M. Stolte, "The new Vienna classification of epithelial neoplasia of the gastrointestinal tract: advantages and disadvantages," *Virchows Arch.* **442**(2), 99-106 (2003)
21. R. D. Odze, "Diagnosis and grading of dysplasia in Barrett's oesophagus," *J. Clin. Pathol.* **59**(10), 1029-1038 (2006)
22. G. W. Falk, "Risk Factors for Esophageal Cancer Development," *Surgery Oncology Clinics of North America* **18**(3), 469-485 (2009)
23. M. Wallace, and P. Fockens, "Probe-Based Confocal Laser Endomicroscopy," *Gastroenterology* **136**(5), 1509-1513 (2009)
24. M. Nakao, S. Yoshida, S. Tanaka, Y. Takemura, S. Oka, M. Yoshihara, and K. Chayama, "Optical biopsy of early gastroesophageal cancer by catheter-based reflectance-type laser-scanning confocal microscopy," *J. Biomed. Opt.* **13**(5), - (2008)
25. R. Kiesslich, L. Gossner, M. Goetz, A. Dahlmann, M. Vieth, M. Stolte, A. Hoffman, M. Jung, B. Nafe, P. Galle, and M. F. Neurath, "In Vivo Histology of Barrett's Esophagus and Associated Neoplasia by Confocal Laser Endomicroscopy " *Clin. Gastroenterol. Hepatol.* **4**(8), 979-987 (2006)
26. K. Dunbar, P. Okolo, E. Montgomery, and M. Canto, "Confocal laser endomicroscopy in Barrett's esophagus and endoscopically inapparent Barrett's neoplasia:

a prospective, randomized, double-blind, controlled, crossover trial," *Gastrointest. Endosc.* (2009)
27. D. Li, W. Zheng, and J. Qu, "Imaging of epithelial tissue in vivo based on excitation of multiple endogenous nonlinear optical signals," *Opt. Lett.* **34**(18), 2853-2855 (2009)
28. B. Lin, S. Urayama, R. M. G. Saroufeem, D. L. Matthews, and S. G. Demos, "Real-Time Microscopic Imaging of Esophageal Epithelial Disease with Autofluorescence under Ultraviolet Excitation," *Opt. Express* **17**(15), (2009)
29. B. Lin, S. Urayama, R. M. G. Saroufeem, D. L. Matthews, and S. G. Demos, "Endomicroscopy imaging of epithelial structures using tissue autofluorescence," *J. Biomed. Opt.* **16**(046014 (2011)
30. S. G. Demos, C. A. Lieber, B. Lin, and R. Ramsamooj, "Imaging of tissue microstructures using a multimodal microscope design," *IEEE J. Sel. Top. Quant.* **11**(4), 752-758 (2005)
31. B. Lin, S. Urayama, R. Saroufeem, D. Matthews, and S. Demos, "Characterizing the origin of autofluorescence in human esophageal epithelium under ultraviolet excitation," *Opt. Express* **18**(20), 21074-21082 (2010)
32. B. Lin, S. Urayama, R. M. G. Saroufeem, D. L. Matthews, and S. G. Demos, "Characterizing the origin of autofluorescence in human esophageal epithelium under ultraviolet excitation," *Opt. Express* **18**(20), 21074-21082 (2010)
33. J. W. Tunnell, A. E. Desjardins, L. Galindo, I. Georgakoudi, S. A. McGee, J. Mirkovic, M. G. Mueller, J. Nazemi, F. T. Nguyen, A. Wax, Q. G. Zhang, R. R. Dasari, and M. S. Feld, "Instrumentation for multi-modal spectroscopic diagnosis of epithelial dysplasia," *Technol. Cancer Res. Treat.* **2**(6), 505-514 (2003)
34. HCUP, "Healthcare Cost and Utilization Project," (2008).
35. R. Saroufeem, "University of California Davis Medical Center, Assist. Clinical Professor GI Pathology," (2009).
36. M. J. Schuchert, and J. D. Luketich, "Barrett's esophagus - Emerging concepts and controversies," *J. Surg. Oncol.* **95**(3), 185-189 (2007)
37. F. P. Peters, M. A. Kara, W. D. Rosmolen, F. J. W. ten Kate, K. K. Krishnadath, J. J. B. van Lanschot, P. Fockens, and J. J. G. H. M. Bergman, "Stepwise radical endoscopic resection is effective for complete removal of Barrett's esophagus with early neoplasia: A prospective study," *Am. J. Gastroenterol.* **101**(7), 1449-1457 (2006)
38. M. J. Schuchert, K. McGrath, and P. O. Buenaventura, "Barrett's Esophagus: Diagnostic Approaches and Surveillance," *Thoracic and Cardiovascular Surgery* **17**(301 - 312 (2005)

Table 1. Pretreatment biopsy classification and microscopically observed histologic abnormalities of the esophagus

Pathology diagnosis	Histologic Architecture	Cytology	Optical Image Morphology
BE no dysplasia	• May have regular villous appearance of the surface epithelium	• Enterocytes and goblet cells. • Regular basal oriented nuclei without significant nuclear atypia	• Honeycomb-like pattern of columnar mucosa with goblet cells. • Goblet cells appear as round dark or bright features approximately 10 µm in diameter with or without mucin content, respectively.
Indefinite for dysplasia	• May have regular villous appearance of the surface epithelium	• Same as above with nuclear atypia not extending to surface	• Polypoid-like projections similar to the gastric mucosa
Low grade dysplasia	• Same as above minimal glandular irregularity	• Nuclear enlargement, high N/C ratio, hyperchromasia, pseudostratification extending to the surface • Goblet cell depletion	• Moderately disorganized tissue with loss of the specific cellular outline patterns characteristic of normal squamous or columnar epithelia • Projections obscuring the flat surface of normal mucosa • Glandular crypts are visible as depressions or large dark holes on the surface of columnar epithelium
High grade dysplasia	• Irregularity and nodularity of the surface epithelium • Irregular complex crypt architecture with back to back glands and cribriforming	• More severe hyperchromasia pleomorphism, and nuclear membrane irregularity • Prominent large nucleoli • Loss of nuclear polarity	• The mucosal surface is transformed into multiple papillary, villiform or cauliform structures • Surface becomes more three-dimensional containing 3-D globular features • Villi are recognized from visualization of their characteristic contour
Malignant neoplasia	• Additional highly Irregular angulated glands, cords, nests and single cells infiltrating into the lamina propria (intramucosal carcinoma) and through the muscularis mucosa into the submucosa (invasive adenocarcinoma) • Prominent luminal necrosis	• Nuclear changes more severe than in HGD	• Highly disorganized tissue with loss of the specific cellular outline patterns characteristic of normal squamous or columnar epithelia • Cauliflower-like projections are 10-30 µm in diameter correspond to malignant features • Abnormal blood vascular patterns

Figure Captions

Fig. 1: a) 57 μm x 48 μm section of gold standard H&E image of human esophagus columnar epithelium and b) the corresponding microscopic AF image of a fresh unprocessed biopsy specimen

Fig. 2: a) H&E image of stratified squamous esophageal mucosa, b) corresponding microscopic AF image under 266 nm excitation

Fig. 3: Microscopic AF images of 500 μm x 300 μm section of human biopsy specimens from a) normal duodenum (intestine) mucosa and b) normal cardia (stomach) mucosa. Lines indicate visible microstructures of interest including villi apices (line 1), goblet cells (lines 2 and 3), crypts of Lieberkuhn (line 4).

Fig. 4: 490 μm x 460 μm human esophagus biopsy specimens with a pathology diagnosis of histologically unremarkable squamous esophageal mucosa with very scant columnar components. Arrows indicate observed microstructures believed to be villi crypts.

Fig. 5: 550 μm x 500 μm field of view of a) H&E gold standard cross-section image of esophagus with intestinal metaplasia (BE), and b) the AF image of the corresponding biopsy specimen as image (a). Numbered arrows indicate what could be a goblet cell without mucin (arrow 1), goblet cell with mucin (arrow 2), crypts of Lieberkuhn (arrow 3), and the villi apex of an inflamed gland (arrow 4), that can be visibly correlated in both the H&E cross-section and the AF luminal images.

Fig. 6: AF image of 500 μm x 500 μm sections of human esophagus biopsies specimens of a) BE with reactive atypia, b) BE with moderate acute and chronic inflammation, indefinite for dysplasia. Features indicated with lines 1-4 are consistent with those seen above in Fig. 3(a), possibly representing villous apex, crypts of Lieberkuhn, and goblet cells respectively.

Fig. 7: 521 μm x 397 μm human esophagus biopsy specimens of a) squamocolumnar mucosa with LGD, b) BE with LGD, and c) BE with LGD.

Fig. 8: AF images from 500 μm x 360 μm areas of human esophagus biopsy specimens obtained from different patients that were diagnosed with a) HGD, b) focal adenocarcinoma in a background of high and low grade dysplasia c) EAC, and d) poorly differentiated EAC.

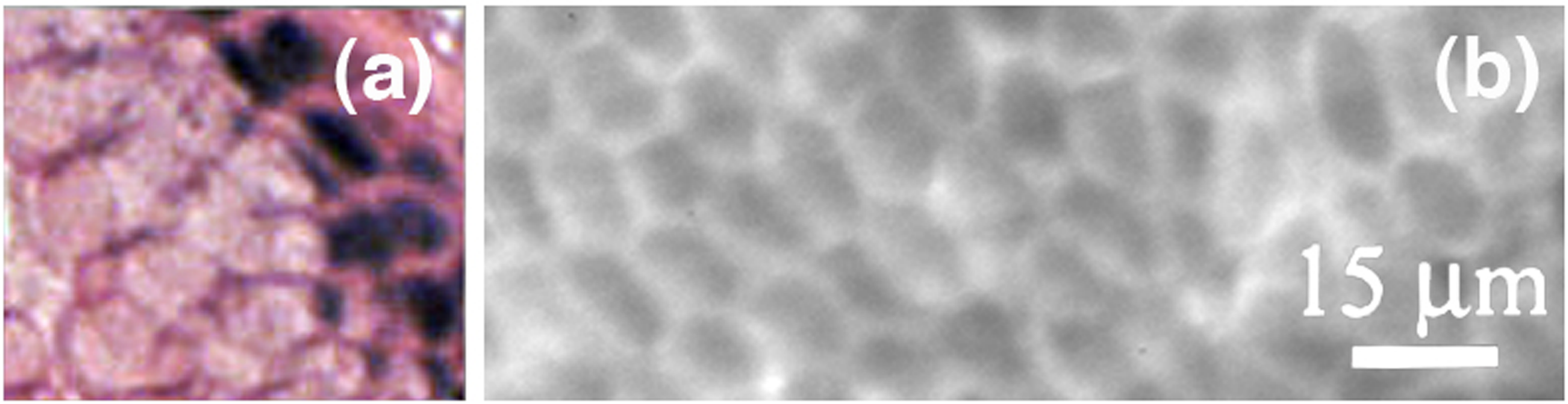

Figure 1

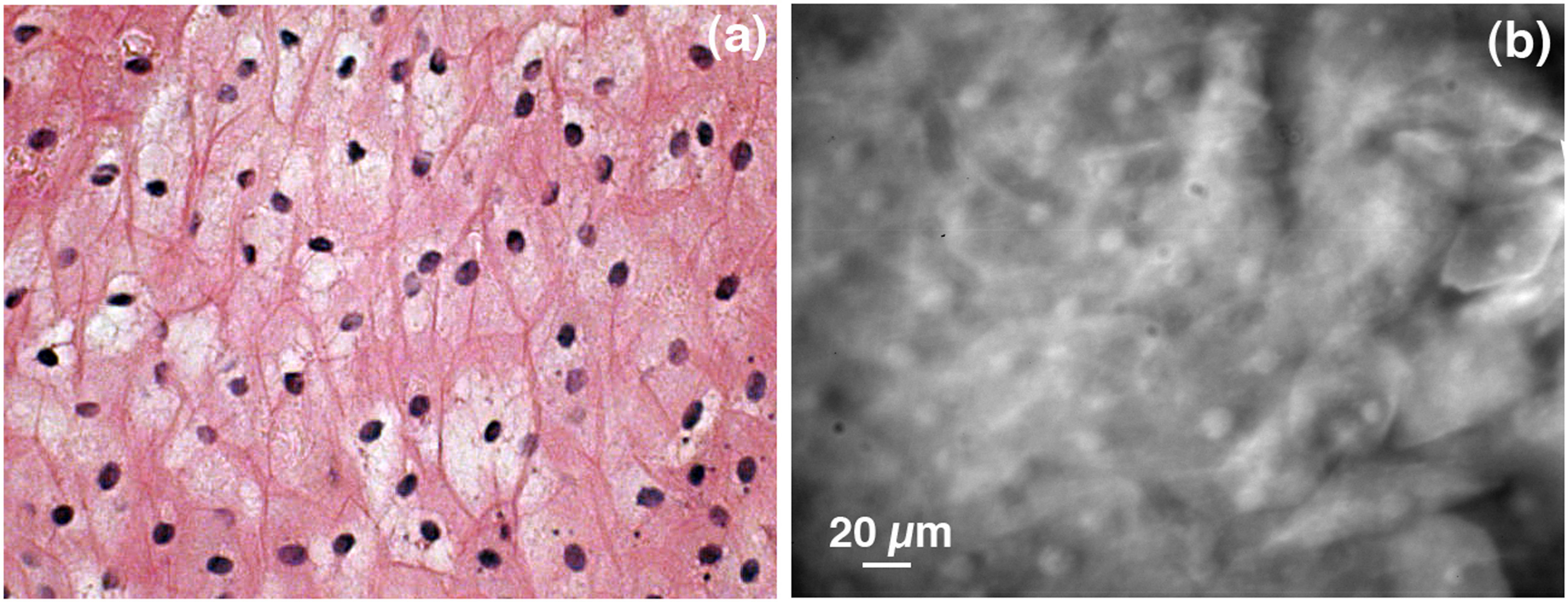

Figure 2

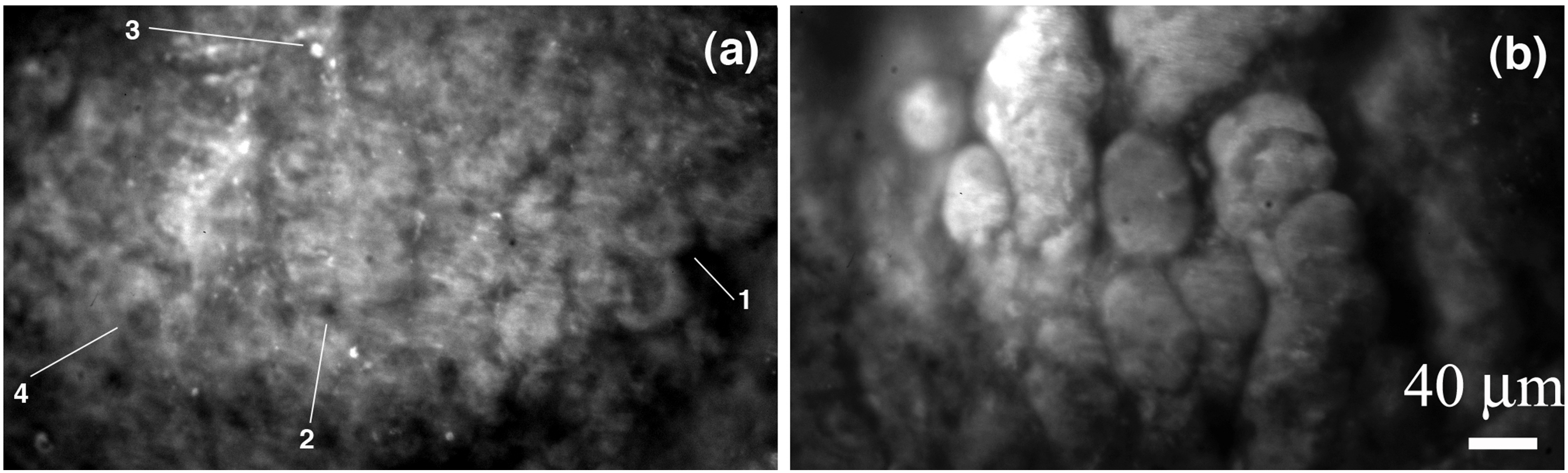

Figure 3

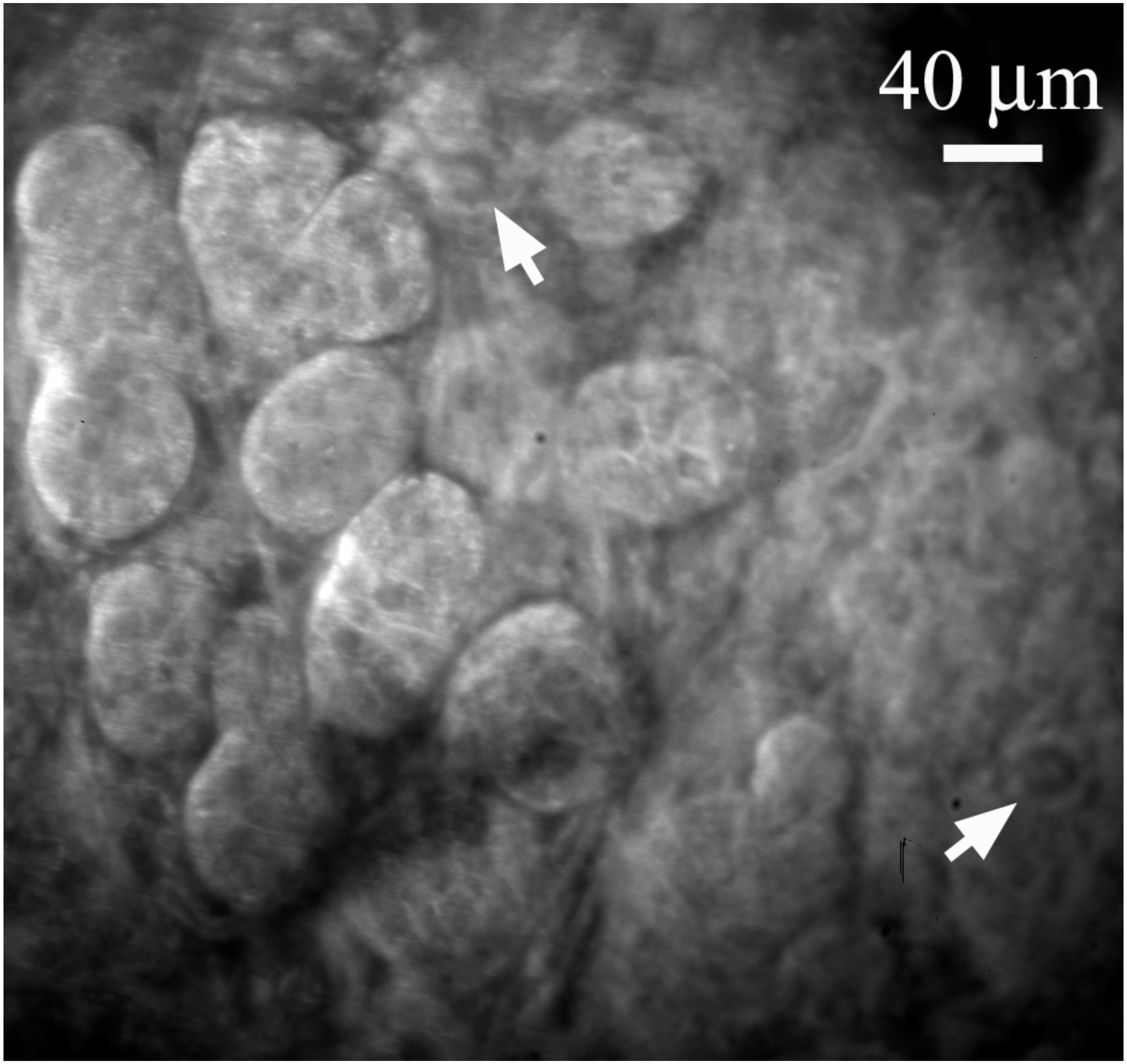

Figure 4

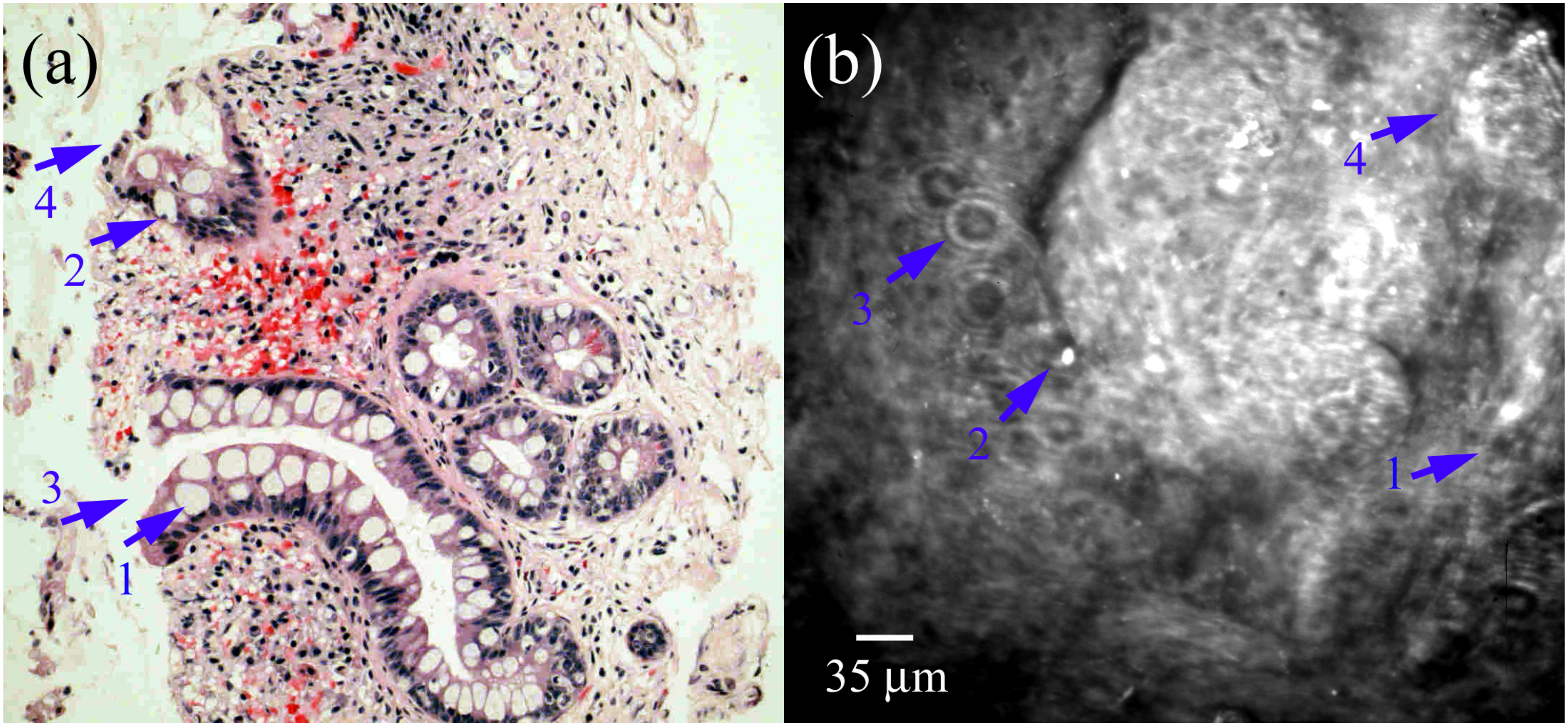

Figure 5

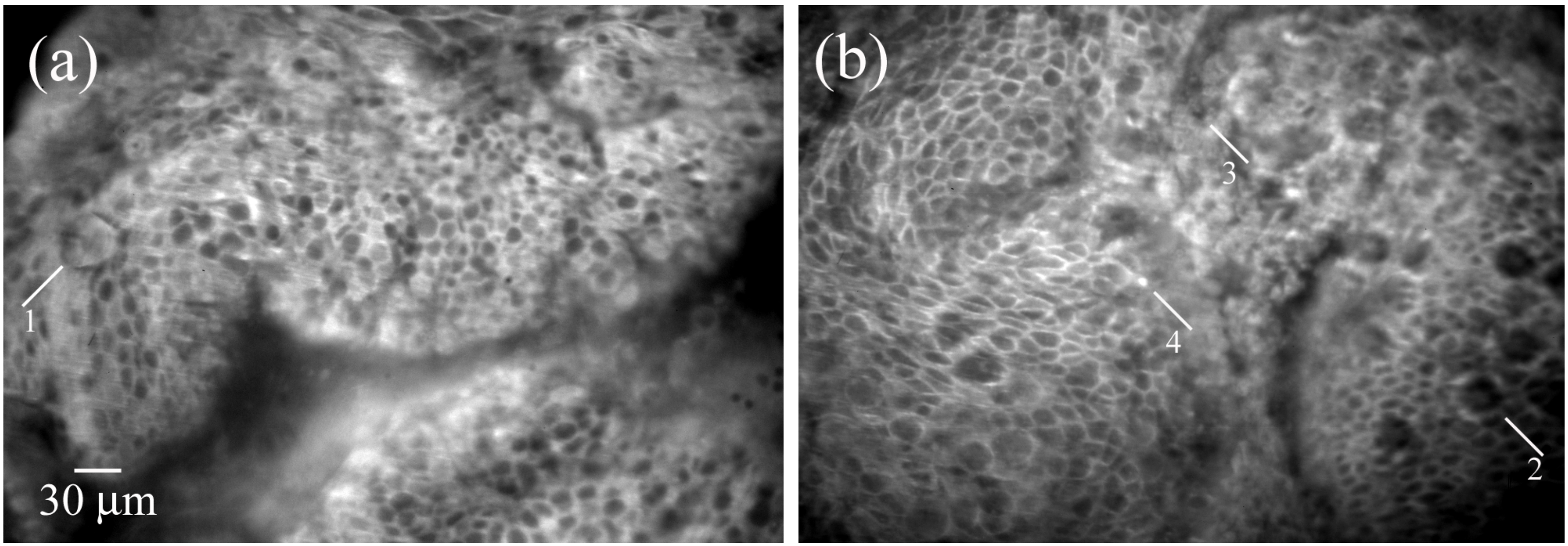

Figure 6

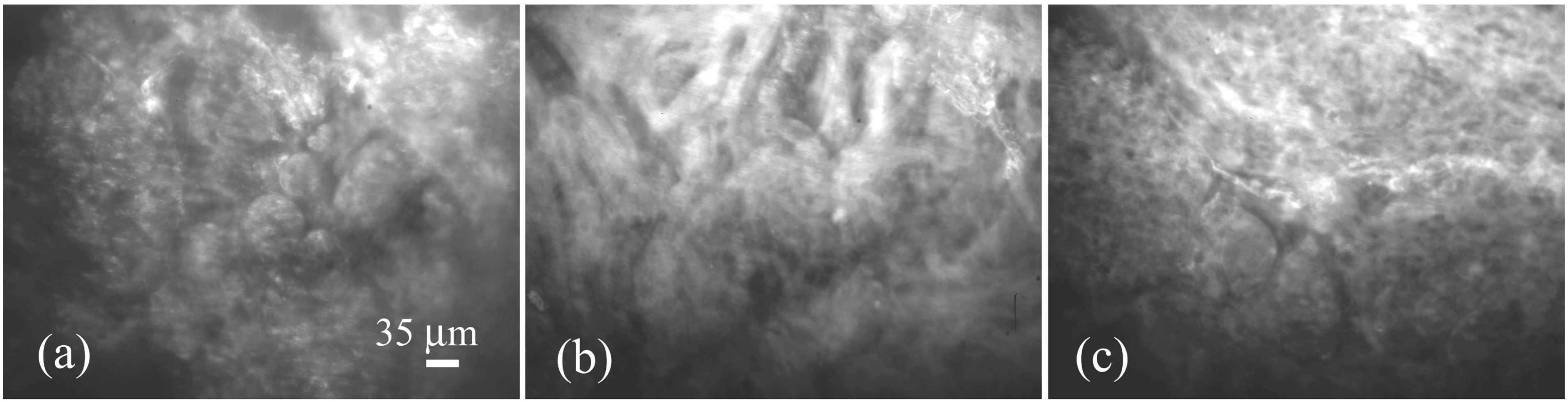

Figure 7

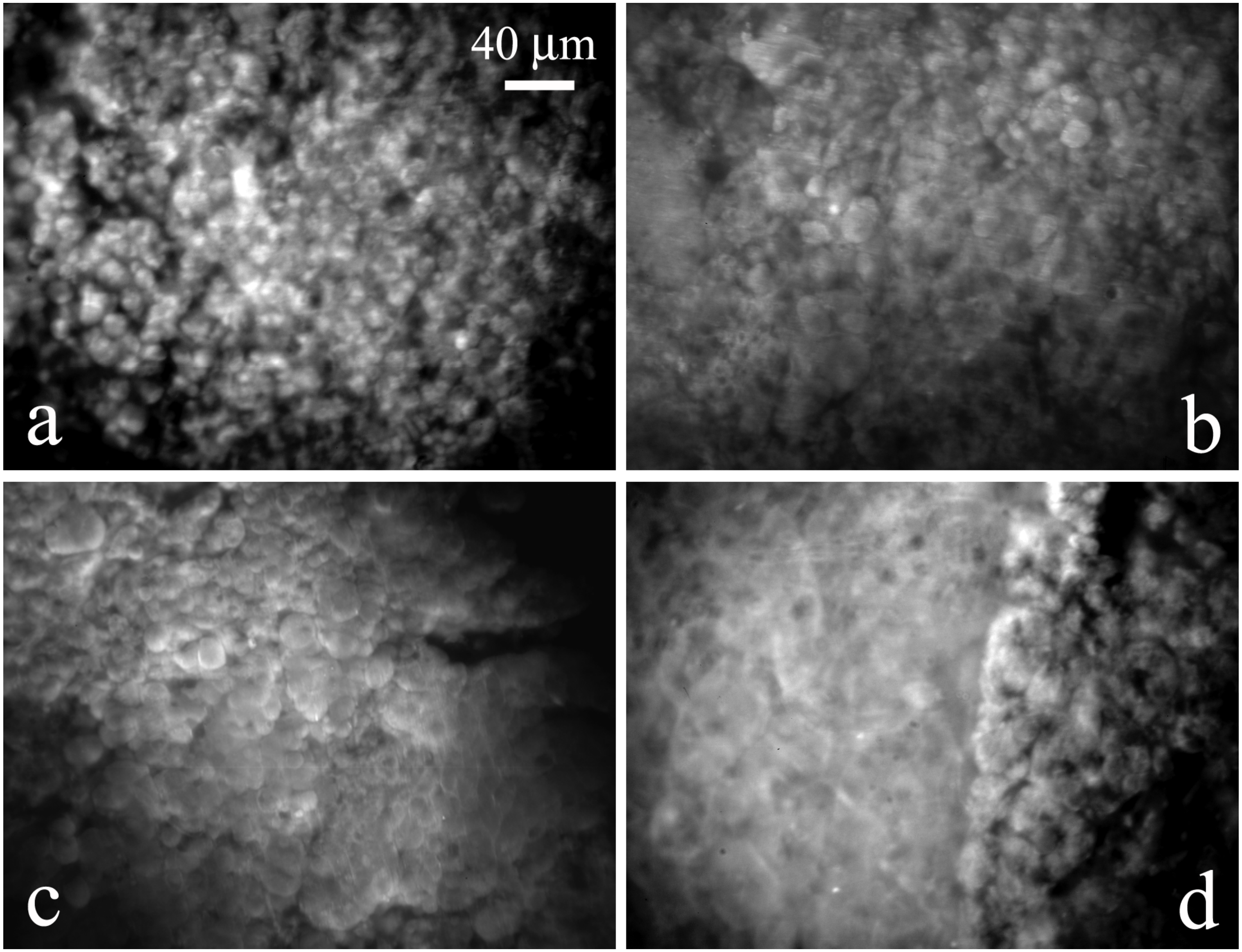

Figure 8